MIT Open Access Articles

THE RISE OF AN IONIZED WIND IN THE NARROW-LINE SEYFERT 1 GALAXY Mrk 335 OBSERVED BY

Massachusetts Institute of Technology

THE RISE OF AN IONIZED WIND IN THE NARROW-LINE SEYFERT 1 GALAXY Mrk 335 OBSERVED BY *XMM-NEWTON* AND *HST*

A. L. LONGINOTTI[1,2], Y. KRONGOLD[3], G. A. KRISS[4,5], J. ELY[4], L. GALLO[6], D. GRUPE[7],
S. KOMOSSA[8], S. MATHUR[9], AND A. PRADHAN[9]

[1] European Space Astronomy Centre of ESA, Madrid, Spain
[2] MIT Kavli Institute, 77 Massachusetts Avenue, Cambridge, MA 02139, USA
[3] Departamento de Astrofisica Extragalactica y Cosmología, Instituto de Astronomía, Universidad Nacional Autonoma de Mexico (UNAM), Apartado Postal 70-264, 04510 Mexico
[4] Space Telescope Science Institute, 3700 San Martin Drive, Baltimore, MD 21218, USA
[5] Department of Physics and Astronomy, The Johns Hopkins University, Baltimore, MD 21218, USA
[6] Department of Astronomy and Physics, Saint Mary's University, Halifax, Canada
[7] Department of Astronomy and Astrophysics, The Pennsylvania State University, 525 Davey Lab, University Park, PA 16802, USA
[8] Max Planck Institut fuer Radioastronomie, Auf dem Huegel 69, D-53121 Bonn, Germany
[9] Department of Astronomy, Ohio State University, 140 West 18th Avenue, Columbus, OH 43210-1173, USA

ABSTRACT

We present the discovery of an outflowing ionized wind in the Seyfert 1 galaxy Mrk 335. Despite having been extensively observed by most of the largest X-ray observatories in the last decade, this bright source was not known to host warm absorber gas until recent *XMM-Newton* observations in combination with a long-term *Swift* monitoring program have shown extreme flux and spectral variability. High-resolution spectra obtained by the *XMM-Newton* Reflection Grating Spectrometer (RGS) detector reveal that the wind consists of three distinct ionization components, all outflowing at a velocity of $\sim$5000 km s^{-1}. This wind is clearly revealed when the source is observed at an intermediate flux state (2–5 $\times$ 10^{-12} erg cm^{-2} s^{-1}). The analysis of multi-epoch RGS spectra allowed us to compare the absorber properties at three very different flux states of the source. No correlation between the warm absorber variability and the X-ray flux has been determined. The two higher ionization components of the gas (log $\xi \sim$ 2.3 and 3.3) may be consistent with photoionization equilibrium, but we can exclude this for the only ionization component that is consistently present in all flux states (log $\xi \sim$ 1.8). We have included archival, non-simultaneous UV data from *Hubble Space Telescope* (FOS, STIS, COS) with the aim of searching for any signature of absorption in this source that so far was known for being absorption-free in the UV band. In the Cosmic Origins Spectrograph (COS) spectra obtained a few months after the X-ray observations, we found broad absorption in C IV lines intrinsic to the active galactic nucleus and blueshifted by a velocity roughly comparable to the X-ray outflow. The global behavior of the gas in both bands can be explained by variation of the covering factor and/or column density, possibly due to transverse motion of absorbing clouds moving out of the line of sight at broad line region scale.

Key words: galaxies: active – galaxies: Seyfert

Online-only material: color figures

1. INTRODUCTION

Outflowing photoionized gas is a well-established feature of over half of all Seyfert galaxies. The presence of this gas is revealed as a series of blueshifted absorption signatures in the spectra of many active galactic nuclei (AGNs) both at UV and X-ray wavelengths (see Crenshaw et al. 2003 for a review).

There are several reasons for keeping our interest high in the study of warm absorbers. The observed velocity shift (almost always to the blue) provides evidence that material is traveling outward from the central region of AGN. If this material eventually leaves the AGN, then outflows might carry significant mass out of the AGN and, as a consequence, give a substantial contribution to the chemical enrichment of the intergalactic medium (IGM; Furlanetto & Loeb 2001; Cavaliere et al. 2002; Germain et al. 2009; Hopkins & Elvis 2010; Barai et al. 2011). The outflow can also impact the development of the host galaxy itself. If it is as strong as 0.5%–5% of the Eddington luminosity of the AGN, then the feedback from the AGN can regulate the growth of the galaxy and the growth of the central black hole as well (Di Matteo et al. 2005; Hopkins & Elvis 2010).

The fact that X-ray absorbers are always found in sources with UV absorption (Crenshaw et al. 2003; Kriss 2006) indicates that there is some interplay between the two phenomena and this in turn implies that photoionized gas must be distributed with high coverage in the AGN.

Several open questions are still awaiting solution. In many cases, high-quality observations of bright sources have allowed us to relate kinematically blueshifted X-ray and UV absorption lines (e.g., Kaspi et al. 2002; Kaastra et al. 2002) leading to the idea of an outflowing wind that spans a wide range of ionization states with a common velocity pattern. In contrast, other cases have shown no obvious relation between UV and X-ray absorption components (Kriss et al. 2011). The ionization structure of the wind was sometimes found to be a continuous distribution, as proposed for NGC 5548 (Steenbrugge et al. 2005) or made by discrete, separate ionization components, sometimes in pressure equilibrium (Krongold et al. 2003), and other times not (Detmers et al. 2011). The location of the photoionized gas is also a subject of debate. The narrow-line region (NLR) on kpc scales (Kinkhabwala et al. 2002), the inner edge of the molecular AGN torus on pc scale (Krolik & Kriss 2001), and the accretion disk on sub-pc distances (Elvis 2000; Krongold et al. 2007) have all been put forward as possible regions of origin for these winds.

One sound piece of evidence that so far has been fully supported observationally is that in the vast majority of

sources—practically 100%—intrinsic absorption is present in both X-ray and UV bands (Crenshaw et al. 2003; Kriss 2006).

The latest *XMM-Newton* and *Hubble Space Telescope* (*HST*) observations of the narrow-line Seyfert 1 Mrk 335 ($z = 0.025785$, Huchra et al. 1999) presented in this paper resolve a potential challenge to this paradigm.

Mrk 335 has a long X-ray history. It has been observed by all the largest facilities throughout the years, with the exception of *Chandra*. The X-ray spectrum has always shown a standard AGN shape: mildly steep power law in the 2–10 keV band, a strong soft X-ray excess and a complex and prominent Fe K line (see Larsson et al. 2008; Longinotti et al. 2007; O'Neill et al. 2007).

Intrinsic soft X-ray absorption was never detected with high confidence. In the *ASCA* survey of warm absorbers presented by Reynolds (1997), this source was not among the list of the ones presenting the characteristic absorption edges that revealed the presence of ionized gas along the line of sight. Likewise, Mrk 335 has never shown any UV absorption either (Zheng et al. 1995; Crenshaw et al. 1999; Dunn et al. 2007).

In 2007, Mrk 335 underwent an abrupt decrease in flux (Grupe et al. 2007, 2008a) and it gave us the opportunity to observe and study a previously unknown emission-line component that revealed the presence of photoionized gas at broad-line region (BLR) scales (Longinotti et al. 2008). The broadband (CCD) spectrum of this peculiar low flux state of Mrk 335 was explained by Grupe and collaborators by an intervening partial covering absorber, although a competing and alternative scenario in which the low state is produced by disk reflection could not be rejected. Noticeably, soft X-ray ionized absorption was not observed in the high-resolution data of any flux state (O'Neill et al. 2007; Longinotti et al. 2008).

In 2009, Mrk 335 was observed for 200 ks by *XMM-Newton* as part of a trigger program based on *Swift* long-term monitoring (Grupe et al. 2012). The source was caught for the first time at a flux state intermediate between the deep minimum of 2007 and the "standard" bright flux in which it was always observed. These data present very different characteristics with respect to previous *XMM-Newton* observations. In particular, they clearly show intrinsic soft-ray absorption in the Reflection Grating Spectrometer (RGS) band. This finding seems to question the one-to-one correspondence reported between X-ray and UV absorbers.

The present paper presents the first high-resolution study of the warm absorber in Mrk 335 and it is based on the comparison of *all* the data obtained through the year 2009 by the RGS spectrometer on board *XMM-Newton*.

The X-ray analysis presented here is complemented by the inclusion of recent and non-simultaneous *HST*-COS spectra that were obtained a few months after the X-ray observations.

2. OBSERVATIONS AND DATA REDUCTION

2.1. XMM-Newton Data

Mrk 335 was observed five times by *XMM-Newton* (see Table 1 for the log of observations). All the data sets were reduced with SAS 11.0.0.[10] For a detailed description of the various data sets, we refer the reader to the numerous prior publications on this source that are listed in Table 1.

The focus of the present paper is the analysis of the warm absorber features in the high-resolution spectra obtained by the

---

[10] http://xmm.esac.esa.int/sas/current/documentation/sas_concise.shtml

Table 1
XMM-Newton Observation Log

ObsID	Date	Exp (ks)	Flux State	Ref
0101040101	2000 Dec 25	37	High	1, 2
0306870101	2006 Jan 3	133	High	3
0510010701	2007 Jun 11	23	Low	4, 5
0600540601	2009 Jun 11	132	Mid	6, 7
0600540501	2009 Jun 13	82	Mid	6, 7

Notes. (1) Gondoin et al. 2002; (2) Longinotti et al. 2007; (3) O'Neill et al. 2007; (4) Grupe et al. 2008a; (5) Longinotti et al. 2008; (6) Grupe et al. 2012; (7) Gallo et al. 2013.

RGS (den Herder et al. 2001), therefore we do not include CCD data from the EPIC MOS cameras, which are extensively described in previous publications. However, the EPIC pn data will be shown and used for measuring fluxes and constraining models, therefore we briefly describe their data reduction in the following.

For all five data sets, the EPIC pn camera (Strüder et al. 2001) was used as prime instrument, and it was operated in full frame mode (0101040101, 0600540501, 0600540601), small window mode (0306870101), and large window mode (0510010701). Data reduction was performed by using the standard tasks *epproc* and *rgsproc*, for pn and RGS data, respectively.

Screening of high particle background was applied to the pn data so as to maximize the signal-to-noise ratio (S/N) according to the procedure described in Piconcelli et al. (2004). The spectral extraction region in the pn camera is a circle of 40 arcsec of radius for source and background spectra, in all observations.

2.1.1. The EPIC pn Data

The CCD data of the *XMM-Newton* campaign are the subject of two more publications presented by our group (Grupe et al. 2012; Gallo et al. 2013). The former paper reports on the long-term variability of Mrk 335, which has been monitored by the *Swift* X-ray Telescope since 2007, and the application of the partial covering model to explain the variation observed by *XMM-Newton*. The latter paper concentrates instead on the analysis of the disk reflection component in the *XMM-Newton* 2009 data.

This complementary work provides the first detailed description of the line-of-sight gas in Mrk 335 as seen by a high-resolution spectrometer, and, as to the X-ray band, it is entirely based on the RGS data. However, consistency between spectral fits performed on the RGS and the EPIC pn data is explored for completeness.

To generally illustrate the dramatic change in the spectral shape of Mrk 335, we have included all the EPIC-pn spectra of Mrk 335 in Figure 1. The 0.3–10 keV figure shows very effectively that the spectral changes are concentrated below 4–5 keV, and that the difference at higher energy is merely attributed to a normalization effect. Continuum fluxes extracted from these spectra are listed in Table 2.

2.2. HST Ultraviolet Spectra

A few months after the *XMM-Newton* observations of Mrk 335 in 2009, the Cosmic Origins Spectrograph (COS) team observed Mrk 335 as part of their program to probe warm and hot gas in and near the Milky Way using AGNs as background sources (Proposal ID 11524; PI: James Green). Green et al.
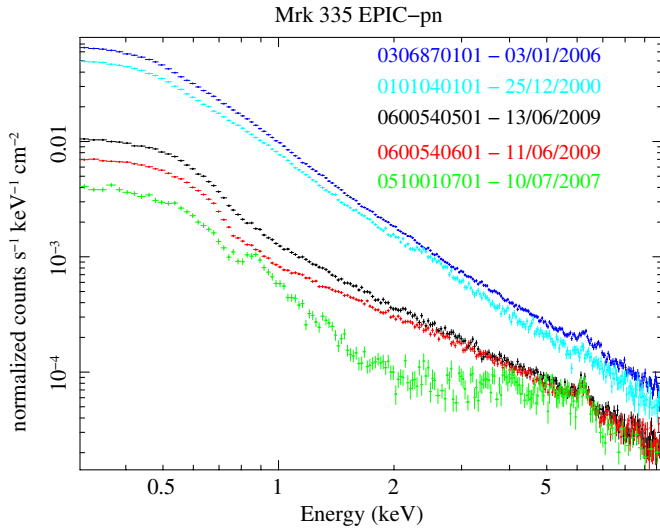
Figure 1. Multi-epoch EPIC pn spectra of Mrk 335. The effective area has been accounted for, therefore the difference between the various observations has to be attributed to intrinsic changes in the spectral shape.

(A color version of this figure is available in the online journal.)

Table 2
X-Ray Fluxes (in units of 10^{-11} erg cm^{-2} s^{-1}) Measured by Fitting the EPIC pn Data with a Broken Power-law Model with Break Energy Fixed at 2 keV

ObsID	Flux (0.3–2 keV)	Flux (2–10 keV)
0101040101	2.60 ± 0.01	1.37 ± 0.01
0306870101	3.32 ± 0.01	1.77 ± 0.01
0510010701	0.20 ± 0.01	0.34 ± 0.01
0600540601	0.36 ± 0.01	0.48 ± 0.04
0600540501	0.52 ± 0.02	0.51 ± 0.05

(2012) describe the key characteristics of the design and performance of the COS instrument on the *HST*. We have retrieved these spectra from the *HST* archive to see if any trace of the unexpected X-ray absorption we see in the RGS spectra has a UV counterpart. Table 3 summarizes the observational details.

The first observation on 2009 October 31 used the primary science aperture and grating G160M with four different central wavelength settings. All four observations used the same focal plane position for the detector, FPPOS = 3. The second observation on 2010 February 12 used gratings G130M and G160M, again with four central wavelength settings for each grating and FPPOS = 3. The four different central wavelength settings provide full coverage across the wavelength gap between segments A and B of the FUV detector. They also place the grid-wire shadows and other detector artifacts at independent places along the spectrum so that they can be more easily removed from the data without gaps in wavelength coverage. We used v12.17.6 of the COS calibration pipeline to process and combine the data. Our processing included a one-dimensional flat-field correction that eliminates the grid-wire shadows and other detector artifacts. The combined G160M spectra cover the wavelength range 1400–1770 Å; the G130M spectrum covers 1135–1440 Å. The G160M spectra each have a median S/N of ∼17 per resolution element. For G130M, the median S/N is ∼33 per resolution element.

Although the COS line-spread function (LSF) has broad wings that can fill in narrow absorption features (Ghavamian et al. 2009), we do not detect any intrinsic lines in Mrk 335 that would necessitate deconvolving the effects of the LSF as in Kriss et al. (2011). Ghavamian et al. (2009) note that the broad LSF has negligible impact on spectral features with Doppler widths exceeding ∼100 km s^{-1}. All spectral features of interest directly related to Mrk 335 have much greater widths.

After processing through the pipeline, we measured the locations of strong interstellar lines in the spectra to determine a zero-point correction for the wavelength scale using the H I

Table 3
HST Observations of Mrk 335

| Data Set Name	Instrument	Grating/Tilt	Date (GMT)	Start Time (s)	Exposure Time (s)
lb4q05010	COS	G160M/1589	2009 Oct 31	13:40:19	408
lb4q05020	COS	G160M/1600	2009 Oct 31	13:50:24	408
lb4q05030	COS	G160M/1611	2009 Oct 31	14:00:29	408
lb4q05040	COS	G160M/1623	2009 Oct 31	14:10:34	409
lb4q06010	COS	G160M/1589	2010 Feb 8	07:34:24	302
lb4q06020	COS	G160M/1600	2010 Feb 8	07:43:02	302
lb4q06030	COS	G160M/1611	2010 Feb 8	07:51:40	302
lb4q06040	COS	G160M/1623	2010 Feb 8	08:00:18	301
lb4q06050	COS	G130M/1291	2010 Feb 8	08:58:05	608
lb4q06060	COS	G130M/1300	2010 Feb 8	09:15:01	605
lb4q06070	COS	G130M/1309	2010 Feb 8	09:28:52	604
lb4q06080	COS	G130M/1318	2010 Feb 8	10:37:38	605
y29e0202t	FOS	H13	1994 Dec 16	05:43:31	1390
y29e0203t	FOS	H13	1994 Dec 16	07:01:06	770
y29e0204t	FOS	H19	1994 Dec 16	07:20:06	960
y29e0205t	FOS	H27	1994 Dec 16	07:40:07	60
y29e0206t	FOS	H27	1994 Dec 16	08:40:19	420
y2gq0301t	FOS	PRISM	1994 Dec 16	08:48:35	60
o8n505010	STIS	E140M	2004 Jul 1	16:24:51	1945
o8n505020	STIS	E140M	2004 Jul 1	17:44:50	2295
o8n505030	STIS	E140M	2004 Jul 1	19:20:49	2875
o8n505040	STIS	E140M	2004 Jul 1	20:56:49	2875
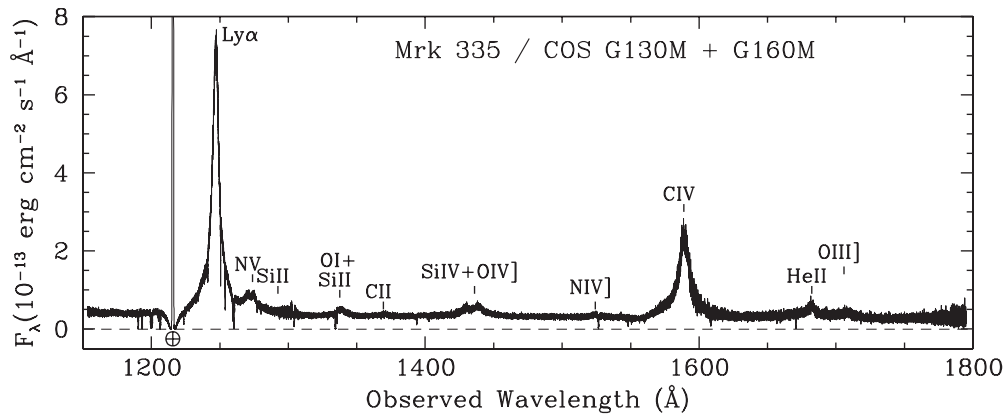
Figure 2. Calibrated COS spectrum of Mrk 335. Wavelengths shortward of 1430 Å are from the G130M observation of 2010 February; longer wavelengths are from the G160M observation in 2009 October. Prominent emission features are indicated. Geocoronal emission in the center of the galactic Lyα absorption trough is indicated with an Earth symbol. The narrow absorption features in the spectrum are either foreground interstellar lines or intervening intergalactic Lyα absorbers.

Table 4
Continuum Fluxes for *HST* Observations of Mrk 335

Observatory	Date	$F(1500\,\text{Å})$ $(10^{-14}\,\text{erg}\,\text{cm}^{-2}\,\text{s}^{-1}\,\text{Å}^{-1})$
HST/FOS	1994 Dec 16	6.0
HST/STIS	2004 Jul 1	3.6
HST/COS	2009 Oct 31	3.1
HST/COS	2010 Feb 8	3.1

velocity of $V_{\text{LSR}} = -11\,\text{km}\,\text{s}^{-1}$ along the Mrk 335 sightline (Murphy et al. 1996). Overall uncertainties in the COS wavelength scale limit our knowledge of the absolute wavelength scale to ~15 km s^{-1}. Figure 2 shows the calibrated COS spectrum of Mrk 335, with the G130M observation from 2010 February merged with the G160M observation of 2009 October.

To place these most recent *HST* spectra in an historical context, we also retrieved archival spectra obtained using the Faint Object Spectrograph (FOS) in 1994, and more recent Space Telescope Imaging Spectrograph (STIS) spectra obtained in 2004. The relevant data sets are also listed in Table 3. For these data we performed no special processing other than to correct the zero point of the wavelength scale of the FOS spectra to align the ISM absorption features with the H I velocity noted above. The STIS spectrum required no additional correction. Table 4 compares the continuum fluxes for all the *HST* observations of Mrk 335 that we discuss below.

3. X-RAY SPECTRAL ANALYSIS

3.1. Strategy

The spectral analysis of the *XMM-Newton* RGS spectra was carried out by using two independent photoionization codes. We applied the *xabs* warm absorber model included in the SPEX fitting package (Kaastra et al. 1996). In parallel, the spectra were analyzed following the same procedure by employing the photoionization code PHASE, developed by Krongold et al. (2003). All the results presented in this paper are extracted from the analysis carried out with the SPEX software. However, the warm absorber properties derived for the 2009 spectra and reported in the following section were fully confirmed by the second analysis. In this way we are confident to have checked the possible model dependency that sometimes is introduced by the use of different photoionization codes.

During the fitting procedure RGS data have been binned by a factor of four. Whenever other choices of grouping were taken (i.e., for plotting purpose), it will be specified. χ^2-statistics was applied and 1σ error bars are quoted throughout the paper.

We highlight our strategy in the following. Since the main purpose of the present work is a detailed study of the warm absorber and its multi-epoch behavior, we start by analyzing the data of 2009, where the presence of the ionized absorber is very evident.

Once a complete model of the ionized gas is established on sound bases for the mid-state, we extend it to the other data sets. In this way we will test the behavior of the absorber at different epochs and its relation to the corresponding flux levels that Mrk 335 has shown during the *XMM-Newton* observations.

Figure 3 displays the comparison of the RGS residuals of the mid- and high-state data fitted by a simple power law and Galactic absorption model. The absorption around 16 Å, which is obvious in the mid-state spectrum observed in 2009, is undoubtedly less pronounced in the high-state data of 2006. Analogously, the emission line around 19 Å is more evident in the mid-state data due to the lower continuum flux with respect to the 2006 spectrum. After this first-order comparison, we proceed to model the absorption observed in the mid-state spectra.

3.2. The Ionized Gas in the 2009 Mid-state

We start by fitting the continuum in the RGS band (7–30 Å) with a power law and a blackbody component to mimic the soft excess. The Galactic column density along the line of sight to Mrk 335 is also included and fixed to $4 \times 10^{20}\,\text{cm}^{-2}$ (Dickey & Lockman 1990).

To this purely phenomenological model of the continuum we added the effect of absorption from ionized material. This effect is modeled by the *xabs* warm absorber code that reproduces the transmission of the nuclear continuum through a slab of ionized gas in photoionization equilibrium. The free parameters in our fits are the column density of the gas, the ionization parameter, the outflow velocity and the root mean square velocity width of the absorption lines. Solar system abundances from Lodders et al. (2009) are assumed.

Initially, the ionized absorber is assumed to be totally covering the source of radiation. Subsequently, in the fitting procedure we will test for the possibility of a more patchy geometry of the gas.
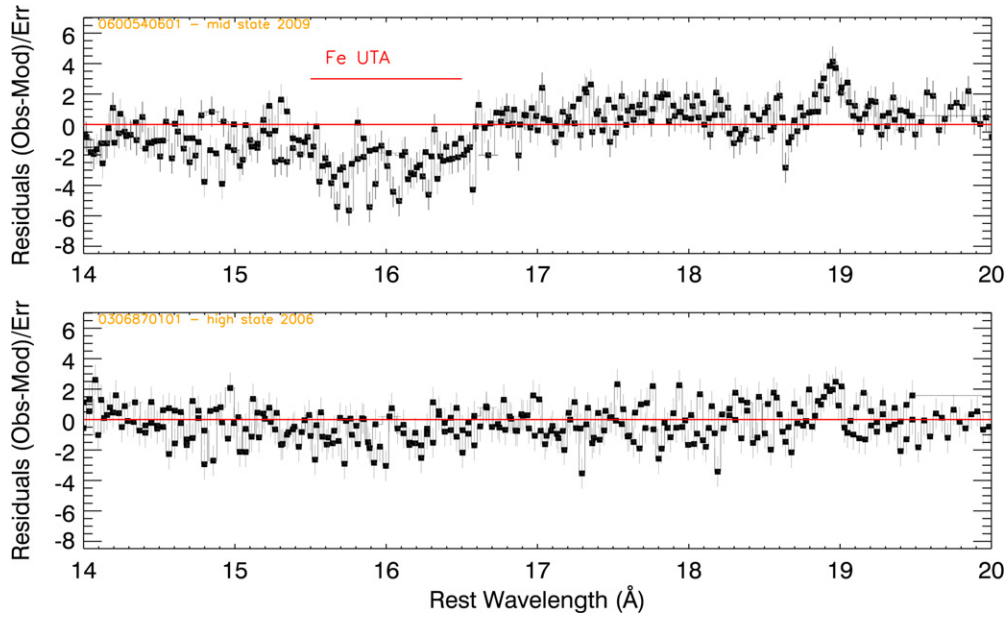
4

Figure 3. Comparison between residuals (in terms of σ) of the mid-state (top) and high-state (bottom) RGS spectrum (ObsIDs 0600540601 and 0306870101) fitted only by a power law and Galactic absorption model. The broad absorption feature produced by the Fe UTA transitions that is very prominent in the mid state disappears almost completely in the high-state data: residuals around 16 Å in the bottom panel are still negative but at a lower significance.

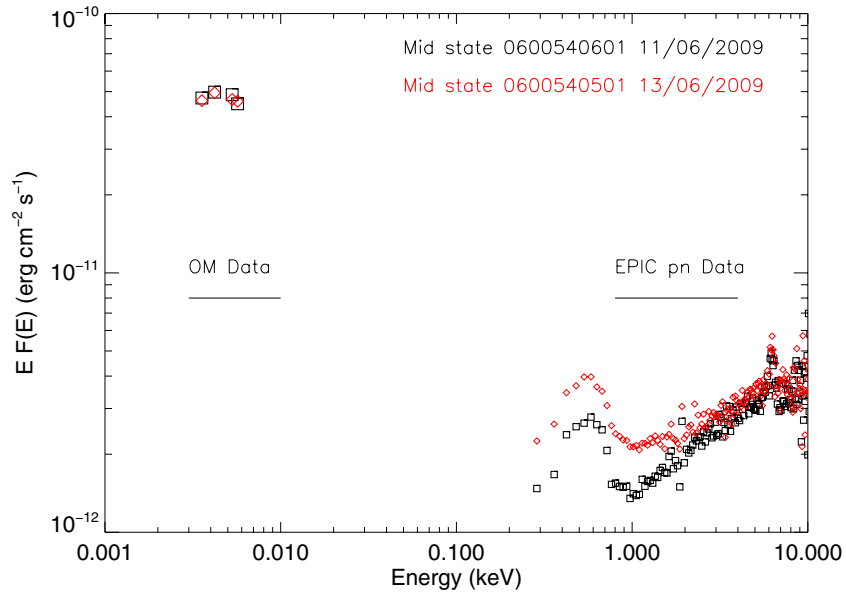(A color version of this figure is available in the online journal.)

Figure 4. Observed spectral energy distribution of Mrk 335 in the 2009 mid-state from *XMM-Newton*.

(A color version of this figure is available in the online journal.)

The absorption spectrum is calculated assuming the photoionization balance produced by the incoming ionizing radiation.

Figure 4 shows the spectral energy distribution (SED) of Mrk 335 including also the data from the optical monitor (OM) on board *XMM-Newton*. The OM observed Mrk 335 in four filters centered at 2182, 2341, 2946, and 3481 Å, simultaneously to the X-ray instruments. This allowed us to add the information on the ultraviolet part of the SED for calculating the ionization balance in our warm absorber models.

Figure 1 and Table 2 show a few percent difference in the soft X-ray flux of the two observations of 2009 (see also Grupe et al. 2012 for the light curve analysis). A visual inspection of the data also reveals little difference in the spectral shape of the two

RGS spectra. We therefore decided to start by carrying out the analysis of the two data sets separately and check consistency in the spectral parameters during the fitting process. All the fit statistics reported below refer to the data set extracted from ObsID 0600540501.

A continuum model without any intrinsic absorption consisting of `Nh Gal *(power law + blackbody)` produces an unsatisfactory fit ($\chi^2/\mathrm{dof} = 1516/1052$).

The addition of one warm absorber component to this baseline model is highly significant ($\chi^2/\mathrm{dof} = 1435/1048$) but still not sufficient to provide a good fit to the spectra. We added a second component and found an improved best-fit model with $\chi^2/\mathrm{dof} = 1334/1044$. When the presence of a third warm

5

Figure 5. RGS spectrum of the 0600540501 mid-state data fitted by the best-fit model in Table 5. The labels of the absorption lines (gray) are blueshifted by an average outflow velocity of 5000 km s^{-1}, the labels for the emission lines (red) correspond instead to the laboratory values. Instrumental features can be distinguished by their typical "squared" shape. The relative contribution of the three warm absorbers is best seen in Figure 6.

(A color version of this figure is available in the online journal.)

Figure 6. Plot of the three (rescaled) warm absorber components detected in the mid-state spectrum and reported in Table 5. From top: medium, high, and low ionization.

(A color version of this figure is available in the online journal.)

absorber was tested the final fit statistics of $\chi^2/\mathrm{dof} = 1307/1040$ was reached. The data fitted by this model are shown in Figure 5. The presence of an additional absorption component that might be postulated after looking at the residuals was tested and found not significant.

The best-fit parameters for the three warm absorbers are summarized in Table 5. The separate contribution of each absorption component to our global model is illustrated in Figure 6. The three models have been renormalized so as to highlight the dominant features in each of them.

3.2.1. Consistency between the Two Mid-state Spectra of 2009

To carefully check the consistency between the two separate *XMM-Newton* observations we applied the warm absorber model described above to the second mid-state data set (ObsID 0600540601). This spectrum is shown in the top panel of Figure 3. In this fit, all the parameters are left free to vary, including those of the baseline continuum model. The detailed results are reported in the second row of Table 5. We concluded that the fit of the two RGS data sets yield parameters fully

Table 5
Best-fit Parameters of the three Warm Absorber Model in the Mid-states of 2009

Data Set	Continuum (T in keV)	Wa Phase	$\log \xi$ (erg cm s^{-1})	Column Density (cm^{-2})	$v_{\rm out}$ (km s^{-1})	$v_{\rm broad}$ (km s^{-1})	χ^2/dof
0600540501	$\Gamma = 2.45^{+0.10}_{-0.17}$	I	$1.92^{+0.05}_{-0.11}$	$2.72^{+1.11}_{-1.03} \times 10^{21}$	4300^{+950}_{-150}	<30	1307/1040
	$kT_{\rm bb} = 0.09 \pm 0.02$	II	$2.35^{+0.24}_{-0.16}$	$4.43^{+2.01}_{-1.30} \times 10^{21}$	5450^{+170}_{-180}	120^{+140}_{-50}	
		III	$3.31^{+0.09}_{-0.08}$	$2.13^{+6.25}_{-1.12} \times 10^{22}$	4000^{+230}_{-180}	170^{+85}_{-60}	
0600540601	$\Gamma = 2.45^{+0.34}_{-0.53}$	I	$1.75^{+0.21}_{-0.35}$	$3.27^{+2.01}_{-2.31} \times 10^{21}$	6000^{+1400}_{-3000}	<70	1249/1033
	$kT_{\rm bb} = 0.11 \pm 0.07$	II	$2.15^{+0.10}_{-0.12}$	$4.80^{+2.30}_{-2.30} \times 10^{21}$	4900^{+160}_{-170}	120^{+60}_{-80}	
		III	$3.22^{+0.55}_{-0.38}$	$2.04^{+40}_{-1.82} \times 10^{22}$	5200^{+650}_{-250}	<650	
First 80 ks	$\Gamma = 2.33^{+0.30}_{-0.50}$	I	1.61 ± 0.16	$3.34^{+1.60}_{-1.35} \times 10^{21}$	4700^{+850}_{-120}	<20	1226/1033
0600540601	$kT_{\rm bb} = 0.10 \pm 0.08$	II	$2.16^{+0.09}_{-0.09}$	$4.07^{+3.40}_{-2.05} \times 10^{21}$	4900^{+160}_{-175}	<70	
		III	$3.26^{+0.17}_{-0.16}$	$4.02^{+18}_{-3.00} \times 10^{22}$	5200^{+1000}_{-200}	90^{+70}_{-55}	
combined RGS	$\Gamma = 2.57^{+1.74}_{-1.91}$	I	$1.85^{+0.04}_{-0.11}$	$2.15^{+0.36}_{-0.26} \times 10^{21}$	4000^{+180}_{-700}	<10	2143/1678
	$kT_{\rm bb} = 0.11 \pm 0.01$	II	$2.11^{+0.02}_{-0.03}$	$4.22^{+0.48}_{-0.48} \times 10^{21}$	5140^{+190}_{-60}	140 ± 30	
		III	$3.19^{+0.05}_{-0.09}$	$3.56^{+1.08}_{-1.82} \times 10^{22}$	5300^{+90}_{-100}	120^{+40}_{-30}	
0600540601 (RGS+ pn)	$\Gamma = 1.76^{+0.02}_{-0.02}$	I	$1.82^{+0.06}_{-0.07}$	$2.86^{+1.78}_{-0.80} \times 10^{21}$	4700^{+170}_{-50}	<15	1704/1284
	$kT_{\rm bb} = 0.11 \pm 0.01$	II	$2.15^{+0.03}_{-0.02}$	$3.62^{+0.22}_{-0.14} \times 10^{21}$	5100^{+90}_{-90}	120^{+40}_{-20}	
		III	3.31 ± 0.13	$6.22^{+2.25}_{-1.12} \times 10^{22}$	6200^{+80}_{-800}	30^{+10}_{-15}	

Notes. The covering factor of the absorbers is fixed to one. The emission lines reported in Section 3.3 are included in these fits.

consistent within the errors. Furthermore, we note that the soft X-ray flux variations between the two observations of 2009 (the 2–10 keV flux being practically constant; see Table 2), does not present variability higher than a 30% level, which is approximately the accuracy in the errors of the detected column densities and ionization parameters (Table 5). Therefore, warm absorber variations induced by the observed flux variability would not be detectable in these data sets.

Nonetheless, we need to consider the results of the variability behavior of Mrk 335 reported by Grupe et al. (2012). These authors have split the data of 2009 according to the pn counting rate and they have obtained two spectra corresponding to "faint" and "bright" portions *within* the 2009 mid-state observations.[11] The "faint spectrum" corresponds to the first 80 ks of obs 0600540601 and it is made by events with less than 3 counts s^{-1}.

In order to exclude that the warm absorber fit is driven by the brightest part of the 2009 data, we have applied the three warm absorbers best-fit model to the RGS spectrum extracted from these 80 ks. The parameters of this fit are reported in the third row of Table 5. In this way we test for possible variations of the warm absorber properties in correlation with the source flux within the 2009 data. The parameters derived in the "faint" 80 ks spectrum are remarkably consistent with those derived when using the two integrated spectra of obs 0600540601 and 0600540501 (first two rows in the table).

We conclude that the ionized gas does not present significant variation while *XMM-Newton* observed Mrk 335 in 2009, therefore we applied the best-fit model to the *combined* data sets of 2009 and from now on, we consider this global data set as "the mid-state." The results from this latest fit are also included in Table 5.

Last, we have checked the effect of the broadband X-ray continuum on our warm absorber model. Indeed, extending the spectral band up to 10 keV might modify the parameters since the power-law slope may not be correctly measured given the

---

[11] In this context "faint and bright" do not have reference to the multi-epoch behavior of the source.

Table 6
Emission Lines Detected in the Mid-state Spectra

ID	λ (Å)	Flux ($\times 10^{-4}$ photons cm^{-2} s^{-1})	$\Delta\chi^2$
O VIII Lyα	18.969	$0.181^{+0.050}_{-0.047}$	33
O VII (r)	21.600	$0.171^{+0.076}_{-0.069}$	14
O VII (i)	21.801	$0.161^{+0.079}_{-0.071}$	12
O VII (f)	22.097	$0.088^{+0.078}_{-0.070}$	3
N VII Lyα	24.779	$0.118^{+0.107}_{-0.099}$	3

Notes. The lines were modeled with a zero-width profile. $\Delta\chi^2$ is quoted for one free parameter.

fact that the RGS band is limited to the soft X-rays (below 2 keV). To this purpose, we have applied the warm absorber model to the RGS and pn data simultaneously. This test was done for ObsID 0600540601. The resulting photon index is indeed modified, being $\Gamma = 1.76 \pm 0.02$ but the warm absorbers properties are basically consistent with the RGS-only-based fit (see Table 5).

3.3. The Emission Lines in 2009

When Mrk 335 was observed at its lowest flux state, Grupe et al. (2008a) and Longinotti et al. (2008) discovered an important emission-line component. Residuals in Figure 3 show a clear emission line corresponding to the position of O VIII Lyα.

To replicate the analysis carried out by Longinotti et al. (2008), we fitted the mid-state data by adding to the three warm absorbers model a series of emission lines with 0-width at the wavelengths listed in Table 6. The wavelengths were kept frozen to the laboratory values in order to allow a direct comparison to the fluxes reported by Longinotti et al. 2008 in their Table 2. Final detections are listed in Table 6. Note that the warm absorber parameters reported in Table 5 and the model plotted in Figure 5 include these emission lines.
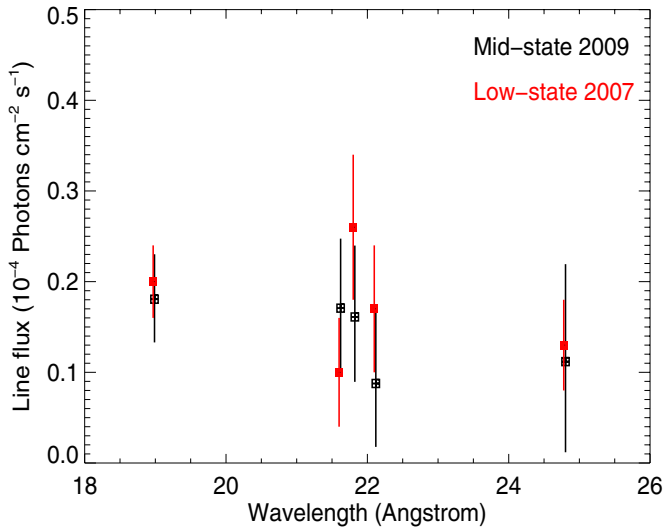
Figure 7. Comparison between the fluxes of the emission lines detected in the mid-state spectrum (black squares) and in the low-state data (red squares). The low-state fluxes are taken from Longinotti et al. (2008). Data points are slightly offset along the *x*-axis for plotting purpose.

(A color version of this figure is available in the online journal.)

Figure 7 shows the fluxes of the emission lines from this work (black points) and from Longinotti et al. (2008; red points). From this figure, it is clear that there is no evidence for variability of the lines' intensity. It is interesting to note that the unusual line ratio of the O VII triplet that led Longinotti et al. (2008) to propose an origin in high-density gas at BLR scale for the line emitting gas is partially confirmed by the new observations. The line ratios measured in the two flux states are consistent within 1σ and, tentatively, this still indicates that the emission lines arise in a high-density gas.

In the low-state spectrum of 2007, it was possible to measure the width of the O VIII Lyα line (FWHM = 0.14 ± 0.05 Å, corresponding to $\sim$2200 km s^{-1}; see Longinotti et al. 2008). This time in the mid-state spectrum we could only obtain a loose upper limit on the width of the same line of 0.58 Å, therefore fully consistent with the 2007 measurement, but still too unconstrained to allow further speculation on the properties of the emitting gas in 2009.

3.4. Multi-epoch Variability and Covering Factor

Once the best-fitting warm absorber model is well established in the mid-state data, we will take it as the reference model for tracing the behavior of the absorber along the other spectral states corresponding to prior epochs. Our aim is to investigate the relation between the ionized gas properties and the flux changes of the source. We propose to carry out this investigation by varying the minimum number of parameters in the best-fit model when this is applied to the other data sets. This way of proceeding will allow us to distinguish which physical parameter is driving the warm absorber variability, if any.

We note here the results reported in Section 3.2.1. *XMM-Newton* observed the source in mid-state within two days in 2009. Despite the moderate flux change, the warm absorber was detected in both spectra with no appreciable change of its properties, but with the present data we cannot exclude that small variations took place on a timescale of days. The consistency of the model found when fitting the two spectra separately (see parameters in Table 5) can only allow us to say that we do not detect short-term variability within the errors.

Before extending our analysis to the other data sets, a final test is carried out on the mid-state spectrum.

3.4.1. The Mid-state Spectrum in 2009: A Partial Covering Warm Absorber?

As a first consideration, we note that so far we have assumed that the ionized gas is distributed to completely cover the X-ray source. In order to test the possibility of a partially covering warm absorber, we have left the covering fraction of the three components free to vary in the fit of the mid-state data. The resulting covering fraction for the low, medium, and high-ionization phases are, respectively, 80%, 75%, and 90%, but they are all consistent with 100%. We could measure error bars only for the covering factor of the low-ionization absorber, which is constrained to 80^{+20}_{-35}%. Hence, the mid-state data are consistent with the presence of a partial covering warm absorber, but this feature is not formally required.

3.4.2. The High-state Spectrum in 2006

The high-resolution spectrum extracted from this epoch at first glance does not suggest the presence of significant absorption (bottom panel in Figure 3), and it is well described by a simple power law with $\Gamma = 2.75 \pm 0.01$. We applied the three warm absorbers model of the 2009 mid-state to these data assuming zero column density, i.e., equivalent to having no absorption. The resulting fit gives χ^2/dof = 1376/1063. If all the absorbers parameters are fixed to the values reported for the mid-state in Table 5, we found, not surprisingly, an unacceptable fit (χ^2/dof = 4502/1063). This result already is an indication that variations have occurred in the ionized gas between the two epochs (2006 and 2009) and we will explore their nature by varying one parameter at a time in each of the three absorber's phases.

1. *Test (a): changes in column density.* We left N_H of the three phases free to vary and kept the other parameters fixed. The resulting model shows that the column density of the gas in the two highest ionization phases (log $\xi \sim$ 2.3 and 3.3) go basically to zero, but the one of the low-ionization phase (log $\xi \sim$ 1.9) is well measured and it is equal to $N_H = 2.72 \pm 0.80 \times 10^{20}$ cm^{-2} with χ^2/dof = 1325/1060. If the ionization parameter of this low-ionization absorber is also left free, we find log ξ = $1.99^{+0.09}_{-0.03}$ and a best fit of χ^2/dof = 1324/1059. This result indicates that the low-ionization phase of the absorber is required by the fit. The gas ionization state is consistent with the mid-state findings but the column density of the absorber in 2006 is found an order of magnitude lower compared to the 2009 measurement (Table 5).

2. *Test (b): changes in the ionization parameter.* As a first test, we fixed the column density to the 2009 values and calculated the ionization parameters that the gas is expected to have if it was in photoionization equilibrium, i.e., we assume that the ionization state of the gas increases with increasing flux, and that the gas responds to the change of the source luminosity in a timescale shorter than the three years elapsed between the two observations. As reported in Table 2, the source flux changed by a factor of $\sim$6.6 between the observations in mid-state (2009) and in high state (2006). Therefore, taking into account the relation of the ionization parameter to the X-ray luminosity $\xi = L/n_e r^2$ and the proportionality between luminosity and flux, we estimate the following ionization states for the

three absorbers under the assumption of photoionization equilibrium: $\log \xi = 2.74$, 3.17, and 4.13 (from the lowest to the highest ionization state, respectively). By forcing the gas to assume these ionization parameters, the fit worsens considerably ($\chi^2/\mathrm{dof} = 2518/1063$). This result shows that a simple picture where the gas is in photoionization equilibrium is not consistent with the data. However, test (a) suggests that some changes in column density occur. Therefore, to test a scenario where the gas is in photoionization equilibrium and at the same time changes in column density, we left N_H free in the three absorbers with ionization parameters fixed to the equilibrium value. None of the absorbers is robustly detected, we find upper limits of $N_H < 1 \times 10^{20}$, 5×10^{21}, 2.8×10^{20} cm^{-2} from the lowest to the highest ionization state. However, the fit ($\chi^2/\mathrm{dof} = 1355/1060$) is worse than the one described in case (a) (where the ionization parameters were fixed to the 2009 values), indicating that at least one of the absorbers is not consistent with being in equilibrium.

3. *Test (c): photoionization equilibrium only in the two highly ionized absorbers*. When the gas reaches a very high ionization state basically no absorption features are produced and the absorber is effectively transparent. For this reason, we cannot yet exclude this possibility in the two highest ionization components since they are always undetected in the high state. To carry out this further test, we left the column density *and* the three ionization states free to vary. In this way, we mainly intended to test the change in ionization of the low-ionization component: in facts, the two higher phases become almost completely ionized and undetectable, in agreement with photoionization equilibrium, but in the low-ionization absorber we found $\log \xi = 1.99 \pm 0.06$ and $N_H = 3.08^{+1.61}_{-0.76} \times 10^{20}$ cm^{-2}.

   This low-ionization component is the only one required by the fit statistics in the high-state data.

4. *Test (d): changes in covering fraction*. As a final test we left the covering fraction of the three phases free to vary as it was done for the mid-state data and described at the beginning of Section 3.4. The model used in this test is the same as the 2009 data and the result is perhaps expected: the high and medium phases are basically transparent with covering factors equal to 0, but the low-ionization phase is required ($\chi^2/\mathrm{dof} = 1338/1057$) with a covering factor of 0.20 ± 0.05.

We conclude that between the high state of 2006 and the mid-state of 2009, two layers of the ionized gas (high and medium ionization) may have changed either ionization state, in agreement with the prescriptions of photoionization equilibrium, or they may have changed covering fraction. The lowest ionization phase of this gas is required to be present in 2009 and 2006, but when the flux increases it does not follow the trend of the other two since also in the high-state data it is detected with approximately the same ionization state as of the mid-state spectrum.

3.4.3. The High-state Spectrum in 2000

For completeness, we repeated the previous analysis on the other high-state data set that is available, the one obtained when the source was observed for the first time by *XMM-Newton* in 2000. This observation was considerably shorter compared to the one in 2006 while the flux level is very similar and the S/N in the RGS spectrum does not allow us to constrain the warm

absorber parameters very tightly. Nonetheless, after repeating the exercise, we can say that the low-ionization phase of the absorber may have been present at this epoch with a coverage of 20%, therefore this spectrum is fully consistent with the 2006 high-state data.

3.4.4. The Low-state Spectrum in 2007

The spectrum extracted from the observation of 2007 corresponds to the lowest flux state observed so far in Mrk 335 (see the green bottom data in Figure 1). For this reason, it is also the one with the lowest S/N in the RGS, which makes the analysis of warm absorber features fairly difficult.

We have taken the same approach described in the previous sections and investigate the presence of the three absorbers in the low-state data. At first, a model without ionized absorption already provides an acceptable fit to the data, with $\chi^2/\mathrm{dof} = 1477/1070$. When we applied the three warm absorber model with parameters fixed to the mid-state best fit, we find a worse fit ($\chi^2/\mathrm{dof} = 1519/1070$). Then, we left the absorbers' column densities free to vary while keeping the ionization states fixed to the mid-state values. This test provides a fit with $\chi^2/\mathrm{dof} = 1480/1067$ and it shows that the column densities of the medium- and high-ionization absorbers go to zero, while the low-ionization one seems to survive, although it is barely detected with a column density of $1.67 \pm 1.10 \times 10^{21}$ cm^2. We calculated the upper limits of the medium- and high-ionization components and they are respectively 8×10^{20} and 1.8×10^{22} cm^2.

The outcome of this test shows that the low-state data are consistent with the presence of an ionized absorber with a low-ionization parameter, but this component is not formally required by the fit.

It should not be surprising that a prior detailed analysis of the high-resolution spectra of the low-state data did not report on the presence of line-of-sight absorption in Mrk 335 (Longinotti et al. 2008). We recall that when the source was observed in 2007 and the data were subsequently analyzed and studied, there was no recognition of the presence of warm absorption in this source so that, given also the meagreness of these data, discarding an in depth analysis of intrinsic absorption seemed a reasonable choice.

We will discuss the implications of the results described in this section after presenting the results from the *HST* analysis.

4. ANALYSIS OF THE *HST*-COS SPECTRA

As a first step in searching for absorption features in the COS spectrum that might correspond to the X-ray absorption observed with *XMM-Newton*, we examine the COS spectra in velocity space as shown in Figure 8. No absorption intrinsic to Mrk 335 is immediately obvious in these spectra. All narrow absorption features are either foreground Milky Way interstellar absorption lines or foreground intergalactic Lyα lines. The foreground interstellar lines have velocities near the observed Milky Way H I velocity (Murphy et al. 1996), or coincident with the Magellanic Stream (Fox et al. 2010). Penton et al. (2002) have identified four intergalactic Lyα lines; none of these have counterparts in other ions.

To carry out a more sensitive search for absorption features in the COS spectra of Mrk 335, we first developed a model for the continuum and emission lines so that we could normalize the spectrum and enhance the contrast of any intrinsic absorption features. Since only the COS observation from 2010 February
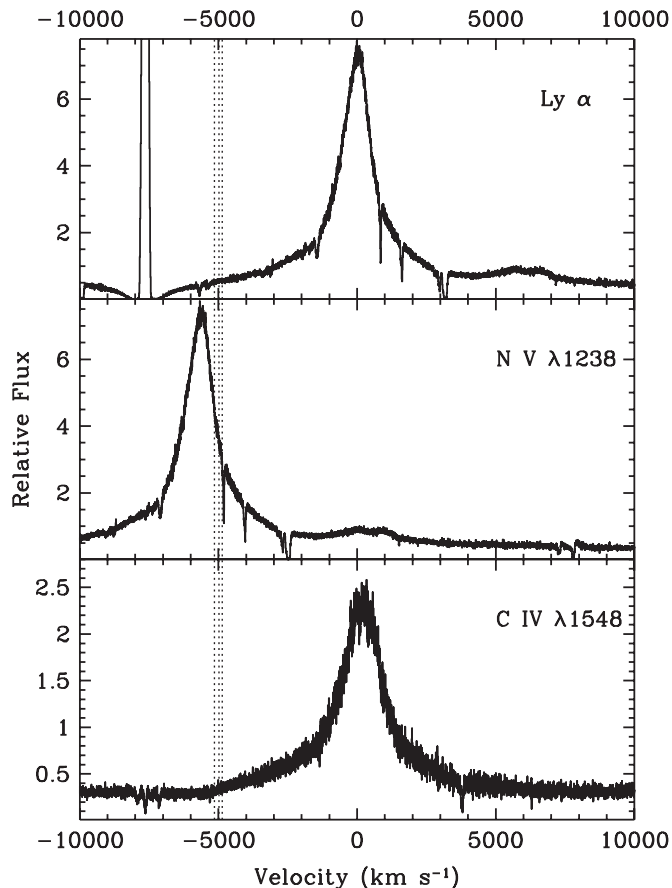
Figure 8. Regions in velocity space in the COS spectra of Mrk 335 surrounding the velocities observed for the absorption features in the *XMM-Newton* mid-state spectra of Mrk 335. Relative fluxes are plotted as a function of velocity relative to the systemic redshift of $z = 0.025785$. The top panel shows velocities relative to Lyα in the COS observation of 2010 February. The middle panel shows the region relative to the N V λ1238 line from the same COS observation. The bottom panel shows the region relative to the C IV λ1548 line from the 2009 October COS observation. Dotted vertical lines indicate the velocities of the absorption components fitted in the *XMM-Newton* spectra.

covered the full FUV spectral range, we started with that observation for our emission model. For the continuum we used a power law, $F_\lambda = F_{1000}(\lambda/1000\,\text{Å})^{-\alpha}$ reddened by $E(B - V) = 0.035$ (Schlegel et al. 1998) using the extinction law of Cardelli et al. (1989) with a ratio of selective to total extinction of $R_V = 3.1$. To get the best fit in the Lyα and C IV regions, we optimized the power-law parameters independently in each spectral region. We used multiple Gaussian components to trace the emission lines. For each line we used the minimum number of components to obtain a good fit. If an additional component improved the fit by a statistically significant amount (>95% confidence using an *F*-test), we included it in our model.

For the narrowest C IV and N V emission lines in Mrk 335, we include contributions from each line in the doublets for each component. We linked the doublet lines so that their wavelengths are in the ratio of their laboratory values. For C IV we assume an optically thin ratio of 2:1 for the fluxes in the blue and red components of the doublets. The optically thin assumption did not provide a good fit for N V, so there we allowed the fluxes to vary independently. For C IV our best fit required an additional very broad component which is not needed in the fits to the Lyα and N V regions. The 13,000 km s^{-1} width of this component is so much greater than the 500 km s^{-1} splitting of the C IV lines

that we did not treat this line as a doublet. We used the IRAF[12] task SPECFIT (Kriss 1994) to do our fits.

Using this same model, we then tried to fit the COS G160M spectrum from 2009 October. Surprisingly, although the spectra look virtually identical at first glance, we found large residuals on the blue wing of the C IV emission line. As shown in Figure 9, there is a shallow, but prominent, depression from 1550 to 1560 Å on the blue wing of the C IV emission line in the 2009 October COS spectrum that is not evident in the 2010 February COS spectrum or in the prior FOS and STIS spectra. As Figure 9 shows, when all four spectra are normalized to the same flux level at 1500 Å, the continuum shape and the base of the C IV line profile appear identical in all regards except for the depression at ~1555 Å that appears in the 2009 spectrum. It is difficult to think of a purely emission model that would account for such a variable feature. We conclude that it is absorption intrinsic to Mrk 335.

To rule out instrumental effects, we examined the four individual spectra obtained at different central wavelength settings on 2009 October 31 and verified that this same feature is present in each one. There are a few bad pixels in this wavelength range in the 1611 central wavelength setting, but these are properly flagged and masked out in the combined spectrum. Observations of the white dwarf spectral standard WD1057+719 from 2009 September to November that bracket the observation of Mrk 335 show only a smoothly varying continuum from 1540 to 1580 Å.

To further test our hypothesis that the spectral feature in the 2009 COS spectrum of Mrk 335 is due to absorption, we have tried several alternative emission models for the base of the C IV emission line and the surrounding continuum. Model I, our best-fit model, is the one we have described above. For Model II, we omit the broad 13,000 km s^{-1} component of C IV that is not present in Lyα or N V. For Model III, we include the low-level forest of Fe II emission lines that are common in AGNs, particularly NLS1s like Mrk 335. Our fit uses the relative intensities of the Wills et al. (1985) Fe II model, and we permit the overall normalization, the line width, and the redshift to vary freely. In our best fit, the Fe II lines have FWHM = 4492 ± 157 km s^{-1} and a velocity relative to systemic of -407 ± 71 km s^{-1}. As summarized in Table 8, Models II and III give dramatically worse fits. For the 2009 October COS spectrum, these models give $\Delta\chi^2 > 100$, and they can be discarded as alternatives to our best-fit model using an absorption feature at >5σ confidence. Again, we conclude that intrinsic absorption is the best description for the unusual feature on the blue wing of the 2009 October COS spectrum of Mrk 335.

For our final best-fit model (Model I) to characterize the C IV absorption in Mrk 335, we exclude the spectral range 1544–1565 Å for our fits to the emission model that we apply to the COS spectra and the other *HST* spectra obtained with FOS and STIS. For these fits we allowed the line and continuum fluxes and line velocities and widths to vary freely. Our best-fit model has a power-law normalization of $F_{1000} = 9.43 \times 10^{-14}$ erg cm^{-2} s^{-1} Å^{-1} with a spectral index of $\alpha = 1.88$. Table 7 gives the parameters of the emission-line components in our model. Figure 10 shows these best-fit emission models for the two COS spectra of Mrk 335 in the C IV region.

---

[12] IRAF (http://iraf.noao.edu/) is distributed by the National Optical Astronomy Observatory, which is operated by the Association of Universities for Research in Astronomy, Inc., under cooperative agreement with the National Science Foundation.
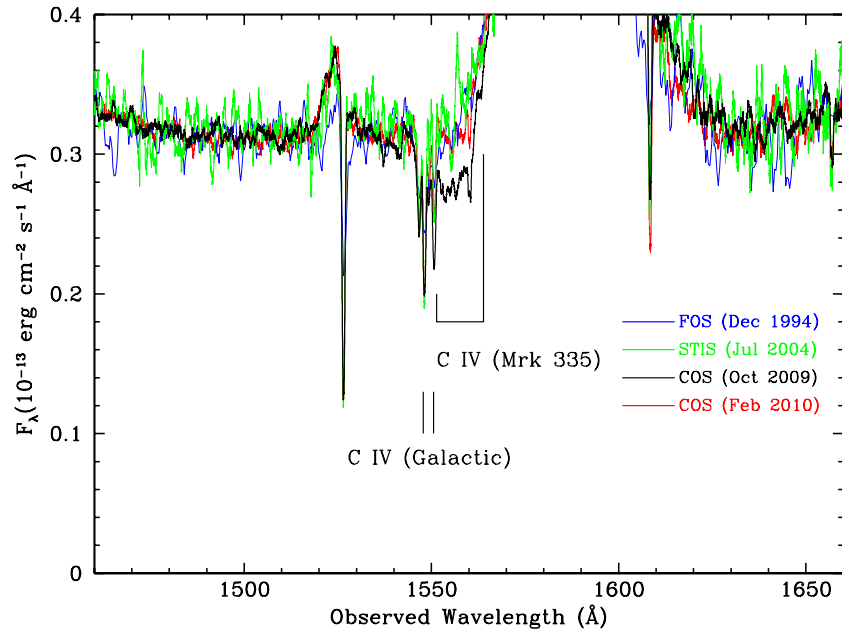
Figure 9. Four *HST* spectra of Mrk 335 in the C IV region. The 1994 December FOS spectrum is in blue, the 2004 July STIS spectrum is in green, the 2009 October COS spectrum is in black, and the 2010 February COS spectrum is in red. We have smoothed the spectra with a running average of 50 km s^{-1} in width. Foreground Galactic absorption due to C IV is marked as is the suspected C IV absorption trough intrinsic to Mrk 335.
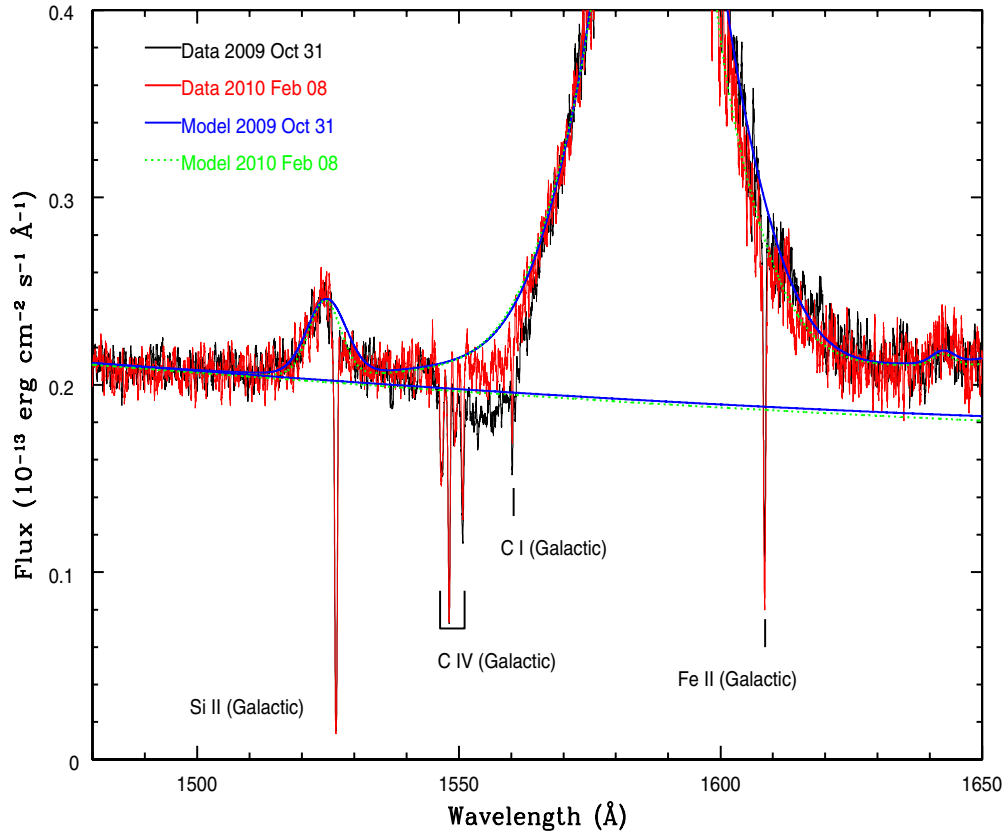
(A color version of this figure is available in the online journal.)

Figure 10. Two COS spectra of Mrk 335 with best-fit models of the continuum and line emission overlaid. The 2009 October 31 spectrum is in black, and the 2010 February 8 spectrum is in red. We have smoothed the spectra with a running average of 50 km s^{-1} in width. The blue and green lines show the fitted power-law continuum and the total fit including all emission-line components.

(A color version of this figure is available in the online journal.)

For a better view of the intrinsic absorption in Mrk 335, we then divided our flux-calibrated spectra by these emission models to produce normalized spectra. Figure 11 shows the normalized spectra for the Lyα, N v, and C IV spectral regions

of the two COS observations. For ease of comparison among the spectra, we have smoothed them with a running average of 50 km s^{-1} in width, or three resolution elements for COS. The most prominent features in each spectrum are the foreground

Table 7
Emission Features in the 2010 COS Spectra of Mrk 335

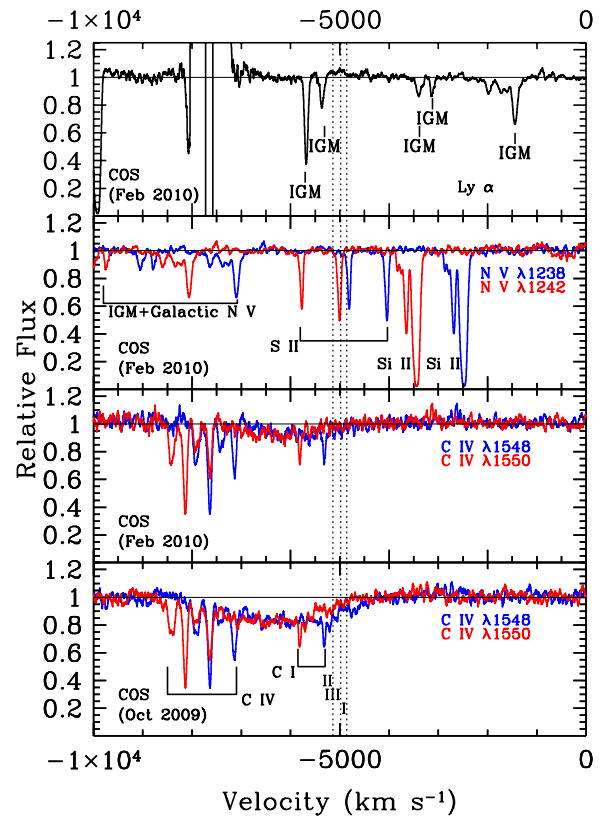| Feature	λ_0 (Å)	Flux (10^{-14} erg cm^{-2} s^{-1} Å^{-1})	v_{sys} (km s^{-1})	FWHM (km s^{-1})
C III*	1175.8	18.0 ± 0.5	353 ± 55	4727 ± 13
Lyα	1215.670	16.8 ± 0.6	63 ± 2	437 ± 17
Lyα	1215.670	175.0 ± 1.2	-25 ± 2	1050 ± 15
Lyα	1215.670	196.0 ± 0.8	20 ± 4	2742 ± 19
Lyα	1215.670	233.0 ± 0.6	-526 ± 8	5976 ± 151
N V	1238.821	7.5 ± 0.2	-8 ± 8	1050 ± 15
N V	1242.804	7.5 ± 0.2	-9 ± 8	1050 ± 15
N V	1238.821	13.0 ± 0.4	-242 ± 4	2742 ± 19
N V	1242.804	6.5 ± 0.2	-242 ± 4	2742 ± 19
N V	1238.821	22.6 ± 0.7	-190 ± 8	5976 ± 151
N V	1242.804	13.3 ± 0.7	-190 ± 8	5976 ± 151
N IV]	1486.496	5.5 ± 0.2	-15 ± 21	1705 ± 61
C IV	1548.195	54.9 ± 1.1	61 ± 9	1119 ± 11
C IV	1550.770	27.5 ± 0.5	61 ± 9	1119 ± 11
C IV	1548.195	35.9 ± 0.5	-178 ± 18	2278 ± 63
C IV	1550.770	18.0 ± 0.3	-178 ± 17	2278 ± 63
C IV	1548.195	93.4 ± 0.3	-124 ± 9	5708 ± 20
C IV	1550.770	46.7 ± 0.1	-124 ± 9	5708 ± 20
C IV	1549.050	26.7 ± 0.8	-1227 ± 9	13263 ± 84
Fe II	1608.450	30.1 ± 0.4	586 ± 71	9992 ± 105
He II	1640.480	8.7 ± 0.2	-103 ± 7	870 ± 19
He II	1640.480	39.3 ± 0.5	-317 ± 28	4954 ± 74
O III]	1663.445	25.6 ± 0.3	368 ± 18	3306 ± 47

Figure 11. Normalized spectra of Mrk 335 in velocity space. Normalized relative fluxes are plotted as a function of velocity relative to the systemic redshift of $z = 0.025785$. The spectra have been smoothed with a running average of 50 km s^{-1} in width. Dotted vertical lines indicate the velocities of the absorption components in the *XMM-Newton* mid-state spectra. The top panel shows the Lyα region of the COS spectrum of 2010 February 8. Here, the IGM Lyα lines identified by Penton et al. (2002) are marked. The second panel shows the N V region of the 2010 February 8 spectrum with N V λ1238 in blue and N V λ1242 line in red. The two bottom panels show the C IV region of the COS spectra of 2010 February 8 and 2009 October 31, respectively; C IV λ1548 is in blue, and λ1550 is in red. The narrow absorption features in each panel are foreground Galactic and IGM lines, which we have labeled.

(A color version of this figure is available in the online journal.)

Milky Way and Magellanic Stream absorbers, as well as the foreground Lyα IGM absorption identified by Penton et al. (2002). In addition, in the 2009 October COS spectrum, *we clearly see the smooth, broad absorption in C IV that is intrinsic to Mrk 335.* This feature may be weakly present in the 2010 February COS spectrum, but we see no counterparts in the Lyα and N V spectral regions.

As confirmation that the broad, blue-shifted C IV absorption present in the 2009 October COS spectrum is real, in Figure 12 we show normalized spectra of the C IV region of all *HST* spectra of Mrk 335. Again, the foreground Milky Way and Magellanic Stream absorbers in C IV and C I λ1560 are the dominant features. Some weak absorption also appears to be present in 2010 February; we see hints of the broad, blue-shifted C IV absorption in the FOS spectrum, but it is absent in the STIS spectrum.

To measure the column density represented by this absorption, or to set upper limits on its presence, and to establish its statistical significance, we used two different models. Given the breadth of the feature, both C IV multiplets are blended together, so we cannot empirically integrate the optical depth across the spectrum to determine the column density and covering fraction. Instead, we fit a model consisting of Voigt profiles for each of the C IV lines, with the column density times the oscillator strength, Nf, set at a 2:1 ratio for the blue versus the red multiplet. We tested two different limits—first, we fixed the covering fraction at unity and fit for the best position, width, and column density; second, we set the column density to a highly saturated value ($N = 5 \times 10^{19}$ cm^{-2}) and allowed the covering fraction to vary freely. To establish the statistical significance of the absorption, we also performed fits with no absorption and allowed all emission components (line and continuum) to vary freely. Table 8 gives the best-fit parameters for each of the *HST* observations. The blueshifted C IV absorption is statistically significant for both COS spectra ($\Delta\chi2 = -388.4$ and -70.4) for three additional degrees of freedom for the 2009

October and 2010 February spectra, respectively. For the STIS and FOS spectra, the addition of the absorption component does not produce a statistically significant improvement in the fit, so we only quote 2σ upper limits on the C IV column density for these spectra.

The optically thin case gives the best fit to the COS spectra, which is not surprising, given the smooth profile of the absorption trough. The optically thick, partially covered model has flat-bottomed profiles with sharper sides. As in other AGNs, however, it is also possible that covering fraction varies smoothly with velocity for an optically thick line, but characterizing a case like this would be highly model-dependent for these data given the blending of the C IV multiplets. Although the optically thick case gives a significantly worse fit ($\Delta\chi2 = +31.6$ for 19,667 degrees of freedom), it is statistically acceptable, and it allows a direct comparison to the X-ray models fit to the *XMM-Newton* RGS spectra that allow for partial covering.

The weak detection of C IV absorption in the 2010 February COS spectrum suggests that corresponding absorption should be present in Lyα as well as N V. However, each of these absorption troughs fall in regions of the spectrum in which it would be very difficult to disentangle them from other spectral

Table 8
Best-fit Parameters for C IV Absorption in the *HST* Spectra of Mrk 335

Instrument	Date	Model[a]	N(C IV) (cm^{-2})	v_{sys} (km s^{-1})	FWHM (km s^{-1})	f_{cov}	χ^2/dof
FOS	1994 Dec 16	I	$<0.8 \times 10^{14}$	−6503 (fixed)	2602 (fixed)	1.0 (fixed)	875.26/778
FOS	1994 Dec 16	I	5×10^{19} (fixed)	−6503 (fixed)	747 (fixed)	0.03 ± 0.01	876.08/778
FOS	1994 Dec 16	I	0.0 (fixed)	. . .	. . .	. . .	881.52/779
STIS	2004 Jul 1	I	$<0.5 \times 10^{14}$	−6503 (fixed)	2602 (fixed)	1.0 (fixed)	19696.46/18666
STIS	2004 Jul 1	I	5×10^{19} (fixed)	−6503 (fixed)	747 (fixed)	<0.02	19695.35/18666
STIS	2004 Jul 1	I	0.0 (fixed)	. . .	. . .	. . .	19676.12/18667
COS	2009 Oct 31	I	$(4.9 \pm 0.1) \times 10^{14}$	-6503 ± 34	2602 ± 57	1.0 (fixed)	13756.76/19668
COS	2009 Oct 31	I	5×10^{19} (fixed)	-6503 ± 14	747 ± 7	0.15 ± 0.003	13788.39/19669
COS	2009 Oct 31	I	0.0 (fixed)	. . .	. . .	. . .	14368.39/19671
COS	2009 Oct 31	II	0.0 (fixed)	. . .	. . .	. . .	14313.10/19674
COS	2009 Oct 31	III	0.0 (fixed)	. . .	. . .	. . .	14467.21/19671
COS	2010 Feb 8	I	$(1.7 \pm 0.1) \times 10^{14}$	-6010 ± 49	1744 ± 181	1.0 (fixed)	13565.24/19668
COS	2010 Feb 8	I	5×10^{19} (fixed)	-6494 ± 38	731 ± 25	0.06 ± 0.004	13601.12/19667
COS	2010 Feb 8	I	0.0 (fixed)	. . .	. . .	. . .	13635.63/19671
COS	2010 Feb 8	II	0.0 (fixed)	. . .	. . .	. . .	13621.51/19674
COS	2010 Feb 8	III	0.0 (fixed)	. . .	. . .	. . .	13808.96/19671

Note. [a] Model I uses a power-law continuum and a broad base on the C IV emission line, and C IV absorption is treated as a Gaussian in optical depth. Model II uses a power-law continuum and no broad base for the C IV emission line. Model III uses a power-law continuum and a Wills et al. (1985) model for Fe II emission. Best fits for this model prefer no broad base on the C IV emission line.
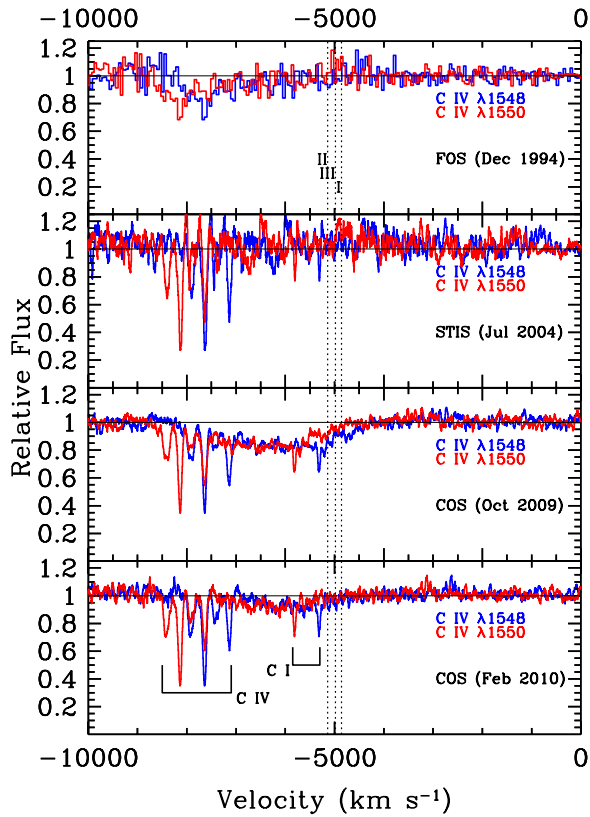

Figure 12. Same as Figure 11 but including all archival *HST* data. From top to bottom: FOS spectrum of 1994 December 16, STIS spectrum of 2004 July 1, COS spectrum of 2009 October 31, and COS spectrum of 2010 February 8. To facilitate the comparison of the spectra from instruments of differing resolution, we have smoothed the spectra with a running average of 50 km s^{-1} in width. Dotted vertical lines indicate the velocities of the absorption components in the *XMM-Newton* mid-state spectra.

(A color version of this figure is available in the online journal.)

features. Referring to Figure 8, note that the Lyα trough falls on the red wing of the damped Lyα absorption from foreground Milky Way gas; the blended N v troughs would roughly be centered on the *peak* of the Lyα emission line of Mrk 335.

Given the breadth of the trough and its similar width to the broad component of the Lyα emission line, a model for the combined absorption and emission is highly degenerate. Our fits show that slight variations in the parameters for the Lyα emission line as well as the damped Galactic Lyα absorption can easily obviate the need for intrinsic absorption. Likewise, absorption comparable to the depth (6% of the continuum intensity) of the C IV absorption observed in the 2010 COS spectrum also provides an acceptable fit.

For completeness, we have fit a model to the 2010 COS spectrum that includes Lyα and N v absorption using the same velocities and widths for the Voigt parameters that provide the best fit to the 2009 October C IV absorption. Formally, the model that *includes* absorption provides a better fit ($\Delta\chi^2 = -19.7$ for 20,079 degrees of freedom and two additional free parameters), but given the strong degeneracy among the components of the model, we simply quote 2σ upper limits on the column densities for H I and N v of $N(\text{H I}) < 7.7 \times 10^{13}\,\text{cm}^{-2}$ and $N(\text{N v}) < 1.0 \times 10^{14}\,\text{cm}^{-2}$ for the 2010 February COS spectrum. A hydrogen column density as high as $1.25\times$ that observed for C IV in the 2010 COS spectrum, $N(\text{H I}) = 2.1 \times 10^{14}\,\text{cm}^{-2}$, gives $\Delta\chi^2 = +20.2$ relative to the best fit. Although significantly worse than the best fit, such a model is statistically acceptable. The lack of strong, obvious Lyα and N v absorption features in the 2010 COS spectrum is not unusual given the weakness of the C IV absorption at this epoch.

5. DISCUSSION

The most recent X-ray and UV observations of Mrk 335 here presented have revealed an unexpected behavior of this complex source.

These observations have provided us with the opportunity to study the emergence of an outflow in a source where this phenomenon was not observed. Among similar cases reported in the literature, we recall the two luminous quasars J105400.40+034801.2 (Hamann et al. 2008) and Ton 34 (Krongold et al. 2010), and the narrow-line Seyfert 1 WVPS 007 (Leighly et al. 2009 and references therein). In all cases the outflow was revealed in the UV broad absorption lines, a

fairly common phenomenon in luminous quasars. The case of WVPS 007 is different since broad absorption is not expected in low-luminosity objects such as this Seyfert 1 type AGN (see Laor & Brandt, 2002). Furthermore, in WVPS 007 the UV out-flow is accompanied by extreme X-ray variability (Grupe et al. 2008b). The new findings on Mrk 335 presented in this work are reminiscent of the behavior of WVPS 007, with the advantage of offering the "X-ray view of the absorber" thanks to its higher X-ray flux.

Warm absorber variability has been extensively observed and studied in several Seyfert 1 galaxies, but in most of the reported cases, the ionized gas has been a constant characteristic of the source, albeit with changing properties.

The presence of ionized gas in Mrk 335 is somewhat elusive in its X-ray records. The results from the *ASCA* survey of AGN published by Reynolds (1997) excluded the presence of ionized absorption in Mrk 335 spectra. Subsequently, observations by high-throughput facilities tend all to confirm the "bareness" of the intrinsic line of sight to this Seyfert galaxy (Bianchi et al. 2001; O'Neill et al. 2007; Larsson et al. 2008).

Quite remarkably, the presence of a variable ionized absorber uncorrelated with the source flux was first proposed in an earlier decade to explain the Ginga spectra of Mrk 335 (Turner et al. 1993). These authors detected a column density around 1.4×10^{22} in the Ginga spectrum of 1987, which was inconsistent with the Ginga data taken the following year.

Since then, we had to wait until the *XMM-Newton* visit of 2009 to observe the ionized gas crossing our line of sight again. The availability of multiple *XMM-Newton* and *Swift* spectra allowed Grupe et al. (2012 and references therein) to propose partial covering from intervening gas as a viable explanation for most of the strong variability exhibited by Mrk 335, albeit an alternative interpretation in terms of blurred reflection remained equally valid to explain the CCD spectra (see also Gallo et al. 2013). Luckily, this time we could rely on the observables measured by a high-resolution spectrometer and reveal the properties of the ionized gas with unprecedented detail.

The analysis presented here favors a solution where the variability of the absorber is related to a change in the column density and/or in the covering fraction of the gas. Changes of the absorber's properties correlated with the flux variability have to be discarded on the basis of test (b) in Section 3.4.2. This test has shown that the ionization parameter expected in photoionization equilibrium for the low-ionization component of the absorber is not consistent with the data. We avoided carrying out the same test in the low-state data (Section 3.4.4) since it already gave a negative response in the data set with the highest S/N: if the ionization parameter was responding to the flux increase, this change would be more likely detected in the RGS spectra of 2006 and our results in Section 3.4.2 have shown that this is not the case.

This lack of correlation therefore points out that the warm absorber overall has little effect on the variability of the continuum.

The results from the *HST* analysis provide us with additional information on the intriguing behavior of this source. Our photoionization models for the X-ray warm absorber in Mrk 335 predict substantial columns of UV-absorbing gas (column densities for Lyα, N V, and C IV are respectively 200, 100, and 30×10^{14} cm^{-2} for the low-ionization component of the X-ray absorber). The column densities measured using COS (see Table 8) are comparable to these predicted column densities, suggesting that the UV absorption we see may be related

to the X-ray absorption. The velocities of the UV absorption troughs are also roughly comparable to the X-ray absorption, but we note that the UV absorption extends to higher velocities and covers a larger total range. In this exercise of comparing the X-ray and UV absorption, we always need to keep in mind that the observations are non-simultaneous, hence the effect of intrinsic variations of these column densities that may occur in between June and (late) 2009 October and 2010 February cannot be taken into account.

Our COS observations show that substantial variations in the C IV absorption can occur on timescales of a few months as well as on timescales of years. If the change in absorption is due to a change in column density, this could be due to either bulk motion of gas or due to an ionization response. However, between 2009 October and 2010 February, there is very little change in the UV continuum flux. Likewise, longer-term UV continuum monitoring using *Swift* shows that UV flux variations in Mrk 335 are only at the level of tens of percent (Grupe et al. 2012). These continuum variations are not strong enough to generate column-density variations as strong as we see.

Therefore, we favor bulk motion of the gas as the best explanation for the absorption variations, which is nicely in agreement with the results from the X-ray analysis.

If the X-ray and UV absorbing gas are rapidly variable and ephemeral, as in Mrk 766 (Risaliti et al. 2011), the absorbers may have moved transversely across our line of sight in the intervening time between the COS observations. Assuming that such motions are due to Keplerian orbits around the central black hole in Mrk 335, we can set limits on the distance of the outflowing gas from the central black hole. For a black hole mass of $2.6 \times 10^7 M_\odot$ (Grier et al. 2012), the minimum size for a cloud that fully covers a disk emitting region of 100 R_G is 4.2×10^{14} cm. For it to move across our line of sight in the 100 days between the two COS observations, the velocity would have to be only 450 km s^{-1}, which would place it at a distance of 3.2×10^{18} cm, slightly exterior to the torus and in the inner NLR. But, at that distance, it would also cover the BLR, which is a few thousand R_G in size. To move across the BLR in that time, the transverse motion would have to be 10–100 times more rapid, more consistent with the outflow velocities of 5000–9000 km s^{-1} seen for the X-ray and UV absorbers. A velocity of 5000 km s^{-1} would be in Keplerian motion at 1.4×10^{16} cm. The BLR in Mrk 335 is at $(0.7–4.7) \times 10^{16}$ cm (Grier et al. 2012; Peterson et al. 2004), so the absorbers would then be in the inner BLR, as suggested for Mrk 766 (Risaliti et al. 2011).

This region was also proposed as a likely location for the X-ray emission lines seen in the low-state spectrum of Mrk 335 (Longinotti et al. 2008). The new data in the mid-state show that the fluxes of the emission lines do not vary significantly (see Section 3.3). Notably, in 2009 we see again a dominant intercombination component with respect to the forbidden line, which seems to confirm the high density of the emitting gas previously postulated (Longinotti et al. 2008). Whether the emitter and the absorber are physically related is difficult to assess without more stringent constraints on the absorber location. The limits on the column densities of the emitting gas derived by these authors in the low-state data are large enough to be consistent with the values measured in this work for the absorbers.

High-velocity transverse motion is a natural explanation for the differences that we have seen in the UV spectra. UV absorbers originating interior to the BLR would be much

REFERENCES

Barai, P., Martel, H., & Germain, J. 2011, ApJ, 727, 54
Bianchi, S., Matt, G., Haardt, F., et al. 2001, A&A, 376, 77
Cardelli, J. A., Clayton, G. C., & Mathis, J. S. 1989, ApJ, 345, 245
Cavaliere, A., Lapi, A., & Menci, N. 2002, ApJL, 581, L1
Crenshaw, D. M., & Kraemer, S. B. 2005, ApJ, 625, 680
Crenshaw, D. M., Kraemer, S. B., Boggess, A., et al. 1999, ApJ, 516, 750
Crenshaw, D. M., Kraemer, S. B., & George, I. M. 2003, ARA&A, 41, 117
den Herder, J. W., Brinkman, A. C., Kahn, S. M., et al. 2001, A&A, 365, L7
Detmers, R. G., Kaastra, J. S., Steenbrugge, K. C., et al. 2011, A&A, 534, A38
Dickey, J. M., & Lockman, F. J. 1990, ARA&A, 28, 215
Di Matteo, T., Springel, V., & Hernquist, L. 2005, Natur, 433, 604
Dunn, J. P., Crenshaw, D. M., Kraemer, S. B., & Gabel, J. R. 2007, AJ, 134, 1061
Elvis, M. 2000, ApJ, 545, 63
Fox, A. J., Wakker, B. P., Smoker, J. V., et al. 2010, ApJ, 718, 1046
Furlanetto, S. R., & Loeb, A. 2001, ApJ, 556, 619
Gallo, L. C., Fabian, A. C., Grupe, D., et al. 2013, MNRAS, 428, 1191
Germain, J., Barai, P., & Martel, H. 2009, ApJ, 704, 1002
Ghavamian, P., Aloisi, A., Lennon, D., et al. 2009, COS Instrument Science Report 2009-01(v1), 1
Gondoin, P., Orr, A., Lumb, D., & Santos-Lleo, M. 2002, A&A, 388, 74
Green, J. C., Froning, C. S., Osterman, S., et al. 2012, ApJ, 744, 60
Grier, C. J., Peterson, B. M., Pogge, R. W., et al. 2012, ApJL, 744, L4
Grupe, D., Komossa, S., & Gallo, L. C. 2007, ApJL, 668, L111
Grupe, D., Komossa, S., Gallo, L. C., et al. 2008a, ApJ, 681, 982
Grupe, D., Komossa, S., Gallo, L. C., et al. 2012, ApJS, 199, 28
Grupe, D., Leighly, K. M., & Komossa, S. 2008b, AJ, 136, 2343
Hamann, F., Kaplan, K. F., Rodríguez Hidalgo, P., Prochaska, J. X., & Herbert-Fort, S. 2008, MNRAS, 391, L39
Hopkins, P. F., & Elvis, M. 2010, MNRAS, 401, 7
Huchra, J. P., Vogeley, M. S., & Geller, M. J. 1999, ApJS, 121, 287
Kaastra, J. S., Mewe, R., & Nieuwenhuijzen, H. 1996, in UV and X-ray Spectroscopy of Astrophysical and Laboratory Plasmas, ed. K. Yamashita & T. Watanabe (Tokyo: Univ. Ac. Press), 411
Kaastra, J. S., Steenbrugge, K. C., Raassen, A. J. J., et al. 2002, A&A, 386, 427
Kaspi, S., Brandt, W. N., George, I. M., et al. 2002, ApJ, 574, 643
Kinkhabwala, A., Sako, M., Behar, E., et al. 2002, ApJ, 575, 732
Kriss, G. 1994, adass, 3, 437
Kriss, G. A. 2006, in ASP Conf. Ser. 348, Astrophysics in the Far Ultraviolet: Five Years of Discovery with FUSE, ed. G. Sonneborn, H. Moos, & B.-G. Andersson (San Francisco, CA: ASP), 499
Kriss, G. A., Arav, N., Kaastra, J. S., et al. 2011, A&A, 534, A41
Krolik, J. H., & Kriss, G. A. 2001, ApJ, 561, 684
Krongold, Y., Binette, L., & Hernández-Ibarra, F. 2010, ApJL, 724, L203
Krongold, Y., Nicastro, F., Brickhouse, N. S., et al. 2003, ApJ, 597, 832
Krongold, Y., Nicastro, F., Elvis, M., et al. 2007, ApJ, 659, 1022
Laor, A., & Brandt, W. N. 2002, ApJ, 569, 641
Larsson, J., Miniutti, G., Fabian, A. C., et al. 2008, MNRAS, 384, 1316
Leighly, K. M., Hamann, F., Casebeer, D. A., & Grupe, D. 2009, ApJ, 701, 176
Lodders, K., Palme, H., & Gail, H.-P. 2009, LanB, 444
Longinotti, A. L., Nucita, A., Santos-Lleo, M., & Guainazzi, M. 2008, A&A, 484, 311
Longinotti, A. L., Sim, S. A., Nandra, K., & Cappi, M. 2007, MNRAS, 374, 237
Murphy, E. M., Lockman, F. J., Laor, A., & Elvis, M. 1996, ApJS, 105, 369
O'Neill, P. M., Nandra, K., Cappi, M., Longinotti, A. L., & Sim, S. A. 2007, MNRAS, 381, L94
Penton, S. V., Stocke, J. T., & Shull, J. M. 2002, ApJ, 565, 720
Peterson, B. M., Ferrarese, L., Gilbert, K. M., et al. 2004, ApJ, 613, 682
Piconcelli, E., Jimenez-Bailón, E., Guainazzi, M., et al. 2004, MNRAS, 351, 161
Reynolds, C. S. 1997, MNRAS, 286, 513
Risaliti, G., Nardini, E., Salvati, M., et al. 2011, MNRAS, 410, 1027
Schlegel, D. J., Finkbeiner, D. P., & Davis, M. 1998, ApJ, 500, 525
Steenbrugge, K. C., Kaastra, J. S., Crenshaw, D. M., et al. 2005, A&A, 434, 569
Strüder, L., Briel, U., Dennerl, K., et al. 2001, A&A, 365, L18
Turner, T. J., Nandra, K., Zdziarski, A. A., et al. 1993, ApJ, 407, 556
Wills, B. J., Netzer, H., & Wills, D. 1985, ApJ, 288, 94
Zheng, W., Kriss, G. A., Davidsen, A. F., et al. 1995, ApJ, 444, 632